Am J Cancer Res 2024;14(5):2626-2642
www.ajcr.us /ISSN:2156-6976/ajcr0156176

Original Article

Efficacy and advantage of immunotherapy for melanoma *via* intramuscular co-expression of plasmid-encoded PD-1 and CTLA-4 scFvs

Yueyao Yang[2*], Qian Huang[1,6*], Mo Cheng[1], Lu Deng[2], Xun Liu[2], Xiufeng Zheng[1], Jing Wei[1], Yanna Lei[1], Xiaoyin Li[1], Fukun Guo[4], Yu Deng[5], Yi Zheng[4], Feng Bi[3], Gang Wang[2], Ming Liu[1]

[1]Department of Medical Oncology/Gastric Cancer Center, West China Hospital, Sichuan University, Chengdu 610041, Sichuan, China; [2]National Engineering Research Center for Biomaterials, College of Biomedical Engineering, Sichuan University, Chengdu 610064, Sichuan, China; [3]Department of Medical Oncology, West China Hospital, Sichuan University, Chengdu 610041, Sichuan, China; [4]Division of Experimental Hematology and Cancer Biology, Cincinnati Children's Hospital Medical Center, 3333 Burnet Avenue, Cincinnati, OH 45229, USA; [5]School of Basic Medical Sciences, Chengdu University, Chengdu 610106, Sichuan, China; [6]Department of Oncology, The Third People's Hospital of Chengdu, Chengdu 255415, Sichuan, China. [*]Equal contributors.

Received February 27, 2024; Accepted May 15, 2024; Epub May 15, 2024; Published May 30, 2024

Abstract: Immunotherapy, in the shape of immune checkpoint inhibitors (ICIs), has completely changed the treatment of cancer. However, the increasing expense of treatment and the frequency of immune-related side effects, which are frequently associated with combination antibody therapies and Fc fragment of antibody, have limited the patient's ability to benefit from these treatments. Herein, we presented the therapeutic effects of the plasmid-encoded PD-1 and CTLA-4 scFvs (single-chain variable fragment) for melanoma *via* an optimized intramuscular gene delivery system. After a single injection, the plasmid-encoded ICI scFv in mouse sera continued to be above 150 ng/mL for 3 weeks and reached peak amounts of 600 ng/mL. Intramuscular delivery of plasmid encoding PD-1 and CTLA-4 scFvs significantly changed the tumor microenvironment, delayed tumor growth, and prolonged survival in melanoma-bearing mice. Furthermore, no significant toxicity was observed, suggesting that this approach could improve the biosafety of ICIs combination therapy. Overall, the expression of ICI scFvs *in vivo* using intramuscular plasmid delivery could potentially develop into a reliable, affordable, and safe immunotherapy technique, expanding the range of antibody-based gene therapy systems that are available.

Keywords: Immunotherapy, immune-checkpoint inhibitors, intramuscular expression, plasmid, melanoma

Introduction

Melanoma is a tumor caused by the malignant transformation of melanocytes in the stroma and can occur in any part of the body [1]. Surgical excision is the primary treatment for early-stage malignant cutaneous melanoma, while systemic therapy, such as molecular targeting or immunotherapy, is the mainstay for advanced-stage disease or cancer that has advanced [2]. Furthermore, melanoma, renal cell carcinoma, and non-small cell lung cancer patients have all benefited enormously from using immune checkpoint inhibitors (ICIs), particularly antibodies against PD-1 and CTLA-4 [3-5]. The first-line systemic treatment for metastatic and unresectable cutaneous malignant melanoma is mainly anti-PD-1 monotherapy (including Pembrolizumab or Nivolumab) and dual immune combination treatment (Nivolumab and Ipilimumab) [6].

Immunotherapies have enjoyed good clinical reputations but are still expensive to most patients. Additionally, the combined application of antibodies will raise the price and immune-related dangers significantly, bringing the demand for novel and safe antibody production methods. Synthetic nucleic acids are revealing information about gene expression *in vivo*, suggesting novel and interesting antibody-drug delivery techniques with significant implications for the treatment of disease. Adenovirus and adeno associated virus (AAV) vectors may pro-

https://doi.org/10.62347/LJNC8404

vide almost the highest level of gene delivery and expression, but their potential biosafety hazards make their clinical applications more concerning and difficult [7-9]. And intratumor injection of oncolytic virus also has biosafety risk and manufacturing complexity [10]. Although mRNA is easier than DNA for intracellular delivery, it has many disadvantages in the treatment of cancers, such as intrinsic instability, synthesis difficulties in 3'-polyadenylation tailing and 5'-methyl guanosine capping, as well as multiple administrations [11]. Plasmid DNA (pDNA), in comparison, has advantages of low immunogenicity, low price, flexible size, and convenience for production, storage, and transport. Compared to conventional protein-based ICI therapeutics, intramuscularly administered plasmids are non-live, non-replicating, and non-integrating, so, muscle cells can function as factories to produce antibody drugs *in vivo* for an extended time. Intramuscular delivery of plasmids is also the safest modality relative to viral and mRNA delivery, and the injection is well tolerated. However, the low delivery efficiency of plasmid has been a long-standing problem. Fortunately, the efficiency of pDNA-based delivery to skeletal muscles has been significantly improved by combining electroporation and Epigallocatechin gallate (EGCG) [12-15].

A single chain fragment variable (scFv) has the characteristics of high penetration, low immunogenicity, short half-life and fast clearance *in vivo*, and no mismatch problem when it is expressed by intramuscularly delivered plasmid for multi-antibody combination therapy [16, 17]. The incidence of grades 3-4 immune-related adverse events (irAEs) is about 59% in the clinical trials of combined anti-PD-1 and anti-CTLA4 applications [18-20]. It has been shown that the higher incidence and severity among irAEs in enterocolitis was related to the Fc fragment in a CTLA-4 antibody [21, 22].

In this study, we focus on the establishment of a preclinical proof-of-concept trial based on the intramuscular pDNA delivery and expression technique. As it has been proved that melanoma is sensitive to anti-PD1 and anti-CTLA4 immunotherapy, the plasmids were constructed to express PD-1 and CTLA-4 scFv *in vivo* for combined therapy of melanoma. By using the efficient intramuscular gene delivery technique and the enhanced muscle-specific synthetic promoter, we anticipate that the blood concentration of plasmid-encoded PD-1 and CTLA-4 scFv could be high enough for effective control of melanoma, thus offering a novel perspective on combined ICI therapy and providing more practical alternatives for efficient, safe, and economic antibody-based tumor therapy.

Material and methods

DNA plasmid construction

The amino acid sequence of mouse CTLA-4 scFv was obtained from UC10-4F10-11 hybridoma cell line, while published cDNA sequences were used to develop mouse PD-1 scFv (EP 1445 264 A1). Gene sequences of Nivolumab and Ipilimumab scFvs were derived from published patents (US 8008449 B2; US 7605238 B2). The genes were cloned into the plasmids of pcDNA3.1(+) (abbreviated as p_{CMV}) and EMS-pcDNA3.1(+) (abbreviated as pSP) (EMS promotor from patent CN 113106094 B), respectively (EMS, Enhanced Muscle Specific promotor). Information of the plasmids was summarized in **Table 1**. The PureLink Expi Endotoxin-Free Maxi Plasmid kit (Invitrogen) was used to purify the plasmids.

Cell culture and transfection

HEK293T, B16F0, Clone-M3, and A375 cell lines were purchased from the Chinese Academy of Sciences Cell Bank. B16F0 and Clone-M3 cells were grown in RPMI-1640 medium supplemented with 10% embryonic bovine serum (FBS) and 1% penicillin/streptomycin (P/S). HEK293T and A375 cells were maintained in Dulbecco's Modified Eagle's Medium (DMEM) supplemented with 10% FBS and 1% P/S. All cell lines were incubated in a humidified incubator at 37°C and 5% CO_2 and maintained at low passage (< 10 passages). During the passage, mycoplasma contamination was routinely detected. All cell lines underwent regular mycoplasma screening, and all experiments were conducted using mycoplasma-free cells. The cell lines have been authenticated within the last 3 years through multiple evaluations, comparing newly acquired data with well-established databases and reference panels. The process ensures the ongoing verification and validation of cell line identities.

Lipo2000 Transfection Reagents (Invitrogen) were used to transfect HEK293T cells with 2.5

Table 1. Characteristics of the plasmids encoding PD-1 and CTLA-4 scFv

Plasmid	Backbone	Promotor	Insertional gene	Cloning site
p_{CMV}	pcDNA3.1(+)	CMV	/	/
pSP	pcDNA3.1(+)	EMS	EMS promotor	*Mlu* I/*Nhe* I
p_{CMV}sig	p_{CMV}	CMV	Igκ signal peptide	*Nhe* I/*Hin*d III
pSPsig	pSP	EMS	Igκ signal peptide	*Nhe* I/*Hin*d III
pPD1-scFv	pSPsig	EMS	Mouse PD-1 scFv	*Nhe* I/*Hin*d III
pCTLA4-scFv			Mouse CTLA-4 scFv	*Nhe* I/*Hin*d III
pNiv-scFv			Nivolumab scFv	*Hin*d III/*Bam*H I
pIpi-scFv			Ipilimumab scFv	*Hin*d III/*Bam*H I
p_{CMV}PD1-scFv	p_{CMV}sig	CMV	Mouse PD-1 scFv	*Nhe* I/*Hin*d III
p_{CMV}CTLA4-scFv			Mouse CTLA-4 scFv	*Nhe* I/*Hin*d III
p_{CMV}Niv-scFv			Nivolumab scFv	*Hin*d III/*Bam*H I
p_{CMV}Ipi-scFv			Ipilimumab scFv	*Hin*d III/*Bam*H I

μg p_{CMV}sig, p_{CMV}PD1-scFv, p_{CMV}CTLA4-scFv, p_{CMV}Niv-scFv, and p_{CMV}Ipi-scFv plasmids prepared in the previous step, respectively. Next, 48 hours after transfection, cell lysates and supernatants were collected for western blot and ELISA analyses, accordingly.

Mouse tumor model

C57BL/6J, DBA/2N, and NOD/scid/IL2rg$^{-/-}$ mice were purchased from the SiPeiFu Biotechnology Company (Beijing, China). All *in vivo* animal procedures were approved by the Biomedical Research Ethics Committee of West China Hospital in Sichuan University, following guidelines from the Association for Assessment and Accreditation of Laboratory Animal Care International (AAALAC). Male C57BL/6J mice or female DBA/2N mice aged 6 to 7 weeks were subcutaneously injected with 1 × 10^5 B16F0 cells or 1 × 10^6 Clone-M3 cells in 100 μL PBS. Two days later, mice were injected with 50 μg of single plasmid or 100 μg of mixed plasmids in 40 μL solution into tibialis anterior (TA) muscle. Peripheral blood mononuclear cells (PBMCs) were isolated from healthy doors using a standardized density gradient with Ficoll paque plus and 5 × 10^6 PBMCs in 100 μL PBS were administered intravenously to 6-week-old female NOD/scid/IL2rg$^{-/-}$ mice on day 7, followed by a dose of 2 × 10^6 A375-Luciferase cells on day 0. Subsequently, the mice were divided randomly into two groups. On day 2, one group of mice received one i.m. dose of 50 μg pNiv-scFv combined with 50 μg pIpi-scFv. The Control group of mice received i.m. one dose of an equimolar amount of pSP-sig. Tumor growth was evaluated 2 to 3 times per week with an electronic caliper. Tumor volumes were calculated with the formula: Tumor volume (mm^3) = [length (mm) × width^2 (mm^2)]/2. Mice were sacrificed when their weight decreased by more than 10% or the tumor volume reached 2,000 mm^3.

L/E/G in situ gene delivery process

Intramuscular gene delivery was administered using a previously established L/E/G protocol [14]. Here, "L" referred to 0.1% (w/v) Pluronic L64 (Sigma-Aldrich), "E" = electrotransfer, and "G" = EGCG. Briefly, 40 μL of mixed solution containing plasmid, L64, and EGCG was injected *in situ* into each side of a mouse TA muscle using a 29-gauge ultra-fine insulin syringe (BD), followed by an electropulse one hour later.

Western blotting analysis

The supernatants and cell lysates of the transfected cells were subjected to SDS-PAGE gel electrophoresis under reducing or nonreducing conditions. Protein bands in the gel were transferred to Immobilon-P polyvinylidene fluoride (PVDF) transfer membranes. The membranes were blocked in TBST containing 5% skimmed milk for 1 hour and incubated at 4°C overnight with a 1:2000 dilution of HRP anti-6 × His tag antibody (Abcam, ab1187). Membranes were washed twice with TBST (TBS with 0.05% Tween 20), dyed with BeyoECL Moon (Beyotime, P0018FS) and imaged with the ChemiDoc Touch Imaging System (Biorad).

Enzyme-linked immunosorbent assay (ELISA)

To analyze the binding of therapeutic antibody to antigens in the cell supernatant, the ELISA adsorption plate (Corning-Costar, 42592) was coated with 100 ng/well of mouse PD-1, mouse CTLA-4, human PD-1, and human CTLA-4 protein, and kept overnight at 4°C. After washing the plate twice with PBST, 1% BSA was added and blocked for 2 hours at 37°C. The cell supernatants were added to the plates in multiple dilutions and incubated at 37°C for 1 hour. The plates were then washed three times and incubated at 37°C for one hour with HRP anti-6 × His tag antibody. The plate was then washed and colored with TMB Two-Component Substrate (Solarbio). The enzymatic process was halted with a 1 N H_2SO_4 solution after 15 minutes incubation in the dark, and optical density was then monitored at 450 nm using a SYNERGY microplate reader (Biotek).

Competitive ELISA was used to determine therapeutic antibody concentrations in serum. The plate was pre-coated with 10 ng/well recombinant human TROP-2 protein (C-6 × His-tag) (novoprotein, C07M). After washing the plate twice with PBST, 100 μL of 1% BSA was added and blocked for 2 hours at 37°C. Then add 50 μL each of the experimental serum or standard, followed by 50 μL of HRP anti-6 × His tag antibody in each well. TMB was used to visualize the HRP-labeled antibody bound to the microtiter plate. The final color depth was negatively correlated with the content of antibody protein in serum.

Concentration of IFN-γ and TNF-α in serum were measured using the IFN-γ 'Femto-HS' High Sensitivity Mouse Uncoated ELISA Kit (Invitrogen, 88-8314-22) and the TNF alpha Mouse Uncoated ELISA Kit (Invitrogen, 88-7324-22) according to the manufacturer's instructions.

Flow cytometry

Mice were sacrificed and tumors were harvested 14 days after intramuscular pDNA delivery. Tumors were cut into small pieces and digested in RPMI-1640 medium with 100 U/ml collagenases I (Sigma, C0130), 400 U/ml collagenase IV (Sigma, C5138), and 30 U/ml DNase I (Roche, 4716728001) at 37°C under continuous slow rotation for 30 minutes. After red blood cell (RBC) lysis, the karyocytes were passed through a second 70 μm cell strainer. Single-cell suspensions were incubated with CD16/CD32 monoclonal antibody (eBioscience, 14-0161-82) to block non-specific binding, and with Fixable Viability Dye eFluo 450 (Thermo Fischer Scientific, 65-0863-14) to label dead cells. Cells were then stained with CD45-Super Bright 600 (eBioscience, 63-0451-80), CD3-FITC (eBioscience, 11-0031-82), CD4-APC (eBioscience, 17-0042-82), and CD8-PerCP-Cyanine5.5 (eBioscience, 45-0081-80) to determine T cell percentage in tumor microenvironment. In another staining experiment, cells were stained for CD45, CD4, and CD25-PerCP-Cyanine5.5 (eBioscience, 45-0251-82) to analyze T-reg cells. After fixation and permeabilization with the Foxp3 staining kit (eBioscience, 00-5523-00), cells were stained with a panel containing antibodies against Foxp3-PE (eBioscience, 12-5773-82).

Blood samples of NOD/scid/IL2rg$^{-/-}$ mice were collected on day 14 and day 21 after PBMCs injection and then stained with Anti-human CD45 BV421 (BD Biosciences, 563879) and 7-AAD Viability Staining (Invitrogen, 00-6993-50). Flow data were acquired on a BD FACS LSRFortessa (BD Biosciences) and analyzed with Flowjo software version 10.4 (Becton, Dickinson and Company, Ashland, OR, USA). Dead cells and doublets were gated out before downstream analysis.

Histology analysis

Hematoxylin and eosin (H&E), immunohistochemistry, and TUNEL staining analyses were performed on C57BL/6J mice bearing B16 tumors. On the 22nd day after intramuscular injection of plasmid, mice were euthanized. The heart, liver, spleen, lungs, kidneys, muscles, and tumors were harvested freshly, followed by fixing in 4% neutral paraformaldehyde solution. After fixation, 4 μm sections were cut from each paraffin-embedded tissue. For immunohistochemistry staining, the sections were stained overnight at 4°C by anti-6 × His tag antibody for muscles and anti-mouse CD3 antibody for tumors. TUNEL staining was performed using the *in situ* cell death detection kit-POD (Roche). Images were taken by a microscope at 100 × magnification (Leica DMI 4000B, Wetzlar, Germany).

In vivo bioluminescent imaging

BALB/c mice were administered 50 μg of pLuciferase using the L/E/G technique.

The bioluminescent image was initiated 14 days after implantation of B16-Luciferase tumor cells and 7 days after implantation of A375-Luciferase, and conducted weekly after that until the endpoint. The mice were intraperitoneally injected 150 mg/kg D-luciferin substrate (P1043, Promega) and maintained under isoflurane gas anesthesia for 5 minutes before imaging. Live luciferase imaging was performed with an IVIS Spectrum (PerkinElmer, USA) 15 minutes after substrate injection. Furthermore, quantification of tumor bioluminescent activity was analyzed with Living Image 4.4 software (PerkinElmer, USA) by taking a 1-s exposure and recording the photos. Bioluminescent activity was presented as photos per second per cm^2 per steradian ($p/s/cm^2/sr$).

Statistical analysis

All statistical analyses were performed using GraphPad Prism Version 7.0 (GraphPad Software, USA). A minimum of n = 5 mice was considered necessary to ensure sufficient power. The obtained data were processed by using a student's t-test or one-way analysis of variance (ANOVA). Survival data was represented by a Kaplan-Meier survival curve and significance was calculated using a log-rank test and one-way ANOVA with correction for multiple comparisons. These data were considered significant if $P < 0.05$ ($*P < 0.05$, $**P < 0.01$, $***P < 0.001$). The lines in all graphs represented the mean value and the error bars represented the standard deviation.

Results

The designed proteins can be expressed in vitro and in vivo

The genes encoding the heavy or light chain variable domain were codon-optimized and then fused to the Kozak and Igk signal sequences to construct the plasmid for the PD-1 and CTLA-4 scFv expression, respectively (**Figure 1A**). EMS is a highly efficient muscle-specific promotor which is based on our team's past research. The detailed information of plasmids carrying PD-1-scFv and CTLA-4-scFv gene driven by CMV/EMS promotor was shown in **Table 1**. To confirm the expression of PD-1-scFv and CTLA-4-scFv *in vitro*, western blotting results identified the 25 KD bands corresponding to the scFv in the p_{CMV}-PD-1scFv and p_{CMV}-CTLA-4scFv transfected cells and supernatants but not in the controls (**Figure 1B**). Firstly, we verified the feasibility of a muscle expression system based a visualization study by pLuc (plasmid expressing Luciferase) intramuscular injection (Figure S1). *In vivo* test showed that PD-1 scFv levels reached a mean of 600 ng/mL in the serum from mice that received 50 μg pPD-1-scFv injection for 14 days and then steadily declined. On day 21, the levels were equivalent to those on day 7, and the expression below those levels was no longer detectable (**Figure 1C**). According to Western blot analysis, the scFv band could be detected in the serum of all mice that received 50 μg pPD-1-scFv but undetectable in the p_{CMV}sig group (**Figure 1D**). Furthermore, muscle tissues at day 22 were collected for evaluating PD-1 scFv and CTLA-4 scFv expression by immunohistochemistry staining. Immunostaining signals were detected in pPD-1-scFv- and pCTLA-4-scFv-injected mice muscle cells (**Figure 1E**). Next, we examined whether the pDNA-encoded PD-1-scFv or CTLA-4-scFv could bind to mouse PD-1 or CTLA-4. It can be seen that the supernatant binding to PD-1 or CTLA-4 was detectable and the signal intensity decreased in gradient with the increase of dilution ratio, suggesting that PD-1-scFv or CTLA-4-scFv expressed in the supernatant had a good binding activity with its corresponding protein in a concentration-dependent manner (**Figure 1F**, **1G**). These findings demonstrated that p_{CMV}-PD-1-scFv and p_{CMV}-CTLA-4-scFv could encode functional mouse PD-1-scFv and CTLA-4-scFv *in vitro* and *in vivo*.

Intramuscular pDNA-encoded immunomodulatory scFv combinations enables retardation of tumor growth in a melanoma tumor model

The purpose of this study was to monitor the therapeutic durability in melanoma models over a long term. Therefore, the tumorigenesis of melanoma was examined *via* subcutaneous implantation of 1×10^5 B16F0 cells per C57BL/6J mouse (Figure S2). The plasmid was intramuscularly injected by L/E/G system two days after B16F0 tumor cells implantation (**Figure 2A**). Mice in the pCombination group showed slower tumor growth and the tumor vol-

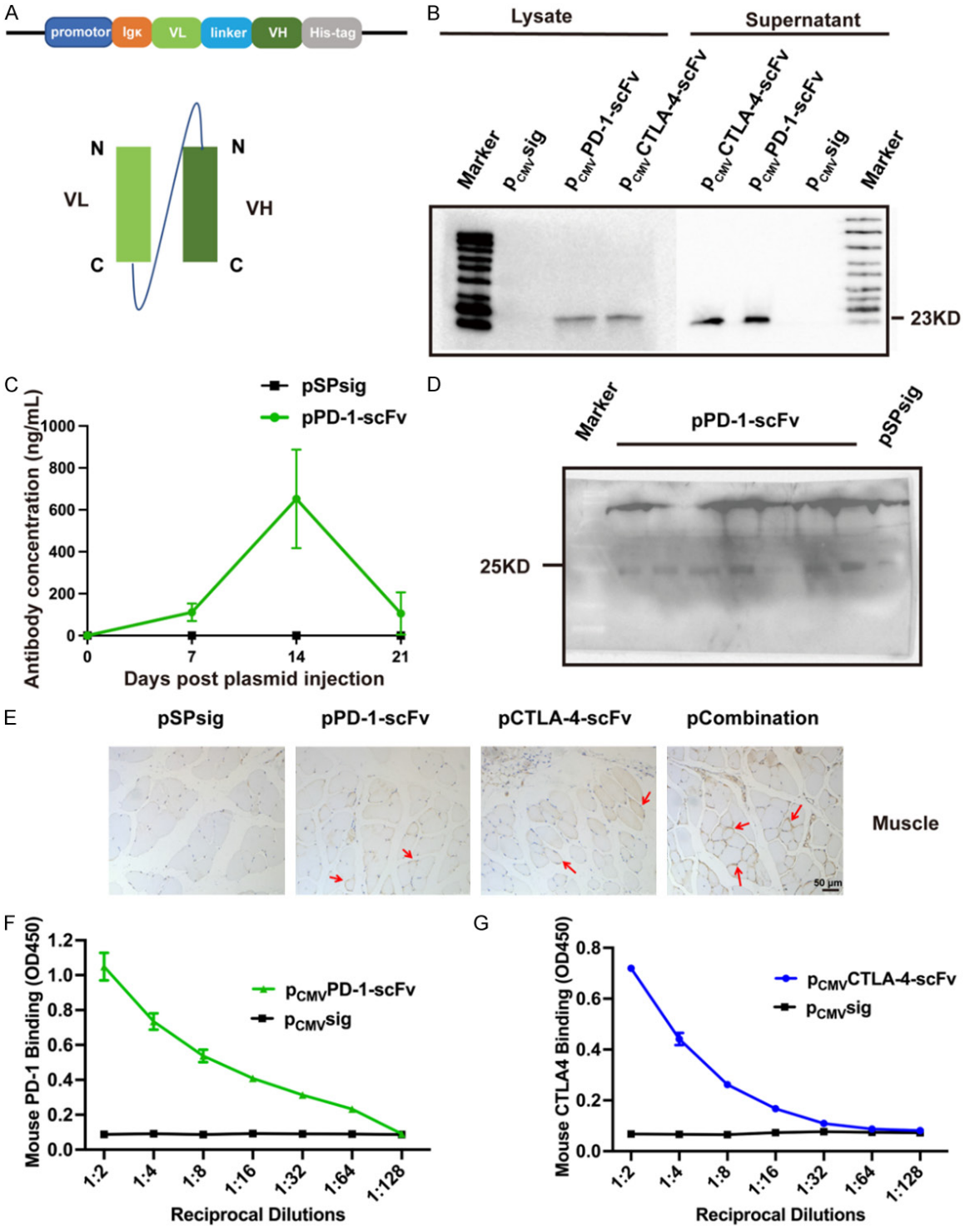

Figure 1. Expression and binding of p_{CMV}PD-1-scFv and p_{CMV}CTLA-4-scFv *in vivo* and *in vitro*. (A) A DNA construct encoding the PD-1 or CTLA-4 scFv. Linker: (G_4S) × 3. Igk: murine Ig kappa-chain signal peptide. (B) *In vitro* expression of PD-1 scFv and CTLA-4 scFv in HEK293T cells detected by Western blot using an anti-6 × His HRP antibody. Time: 48 hours post-transfection. (C) The serum concentration of mouse PD-1 scFv from C57BL/6 mice injected with 50 μg pPD-1-scFv detected by Competitive ELISA. N = 3. (D) PD-1 scFv in mouse serum detected by Western blot 14 days after plasmid (50 μg) injection. N = 8. (E) Immunohistochemical (IHC) staining the expression of PD-1 scFv and CTLA-4 scFv using HRP 6 × His probe in mouse skeletal muscle 21 days post plasmid injection. Scale: 50 μm. Binding of indicated protein with its scFv in culture supernatant from p_{CMV}PD-1-scFv (F) and p_{CMV}CTLA-4-scFv (G) transfected cells 48 hours later, determined by ELISA. Error bars indicated mean ± SD.

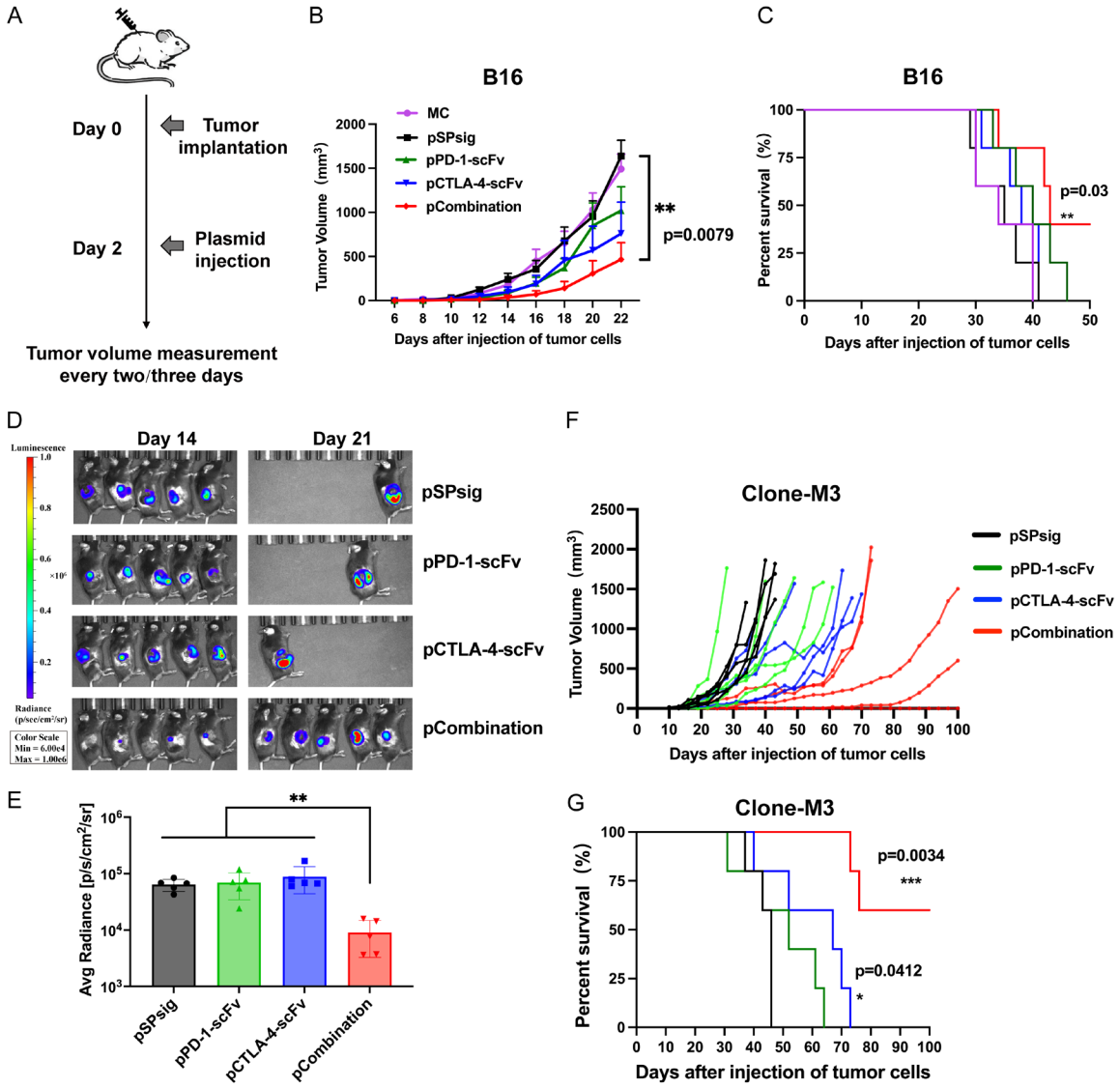

Figure 2. Anti-tumor activity of pPD-1-scFv and pCTLA-4-scFv combination in melanoma model. A. Experiment schema. C57BL/6 or DBA2/N mice were administered subcutaneously 1 × 10^5 B16 or 1 × 10^6 Clone-M3 cells 2 days before intramuscular injection of one dose plasmid. B. Tumor volume. MC: model control without treatment; pSPsig: empty plasmid; pCombination: pPD-1-scFv and pCTLA-4-scFv combination. N = 6. C. Kaplan-Meier Curve showed the mice survival time. D. Bioluminescence imaging (BLI) of mice implanted B16 cells expressing luciferase (B16-Luc). N = 5. E. Average radiance quantification (p/s/cm^2/sr) of BLI at day 14. F. Tumor volume in DBA2/N mice. N = 5. G. Survival curve of DBA2/N mice. Data were plotted as the mean ± SD. The log-rank (Mantel-Cox) test was used to calculate the significance of survival and other statistical significance was calculated using Tukey's multiple comparisons test and one-way ANOVA test. *P < 0.05, **P < 0.01, and ***P < 0.001.

umes were significantly smaller than those in the MC group (**Figure 2B**). The mice survival rate in the pCombination group was also improved as compared with that of other mice (**Figure 2C**). To better monitor the changes in tumors, the experiment was repeated by implanting B16-Luciferease cells (**Figure 2D**). The tumor average radiance value was measured on the 14th day after modeling and the results indicated that the pCombination group had lower bioluminescence values in comparison with other three groups (**Figure 2E**). To confirm further the therapeutic effectiveness, DBA/2N mice were used to inoculate another mouse melanoma cell line Clone-M3. The same treatment mode like B16F0 model was used.

The Clone-M3 tumor growth rate was slower than that of B16F0. In the pCombination group, 1/5 mice were entirely tumor-free, and tumors in 2/4 mice did not reach the tumor volume limitation even on the 100th day (**Figure 2F**). Consequently, pCombination-treated mice acquired an improved survival rate (**Figure 2G**). Taken together, the results confirmed that pDNA-encoded PD-1-scFv and CTLA-4-scFv could exert profound therapeutic effects on melanoma tumor models, providing the possibility of this novel therapy technology for treating human melanoma.

Intramuscular pDNA-based expression of PD-1-scFv and CTLA-4-scFv has adequate biosafety in vivo

During the treatment, there was no statistically significant difference among each group's body weight (**Figure 3A**, **3B**). Next, blood routine and biochemical tests were measured on the 22nd day after plasmid injection. Blood routine tests and biochemical tests are important indicators of reaction safety during the treatment of mice. The blood routine examination showed that the leukocyte cells and the average percentage of neutrophils in the control groups (MC & pSPsig) increased significantly, accompanied by an increased average percentage of lymphocytes in the treatment groups (pPD-1-scFv, pCTLA-4-scFv, pCombination) than those in the control groups, which indicated that mice in the treatment groups had a less leukemoid reaction and inflammatory response (**Figure 3C**). The mice in control groups had noticeably lower hemoglobin levels than reference values but not in the treatment groups, indicating that the treatment alleviated the more severe anemia (**Figures 3D** and S3A). There was no noticeable difference in PLT among the groups (Figure S3B). The results of glutamic oxaloacetic transaminase (AST) and alanine aminotransferase (ALT) were higher in the control groups than those in the treatment groups, suggesting that the treatment improved the liver function (**Figure 3E**). And control group tumors revealed a higher degree of aggressiveness due to a higher LDH level (**Figure 3F**). The blood creatinine concentrations in all groups decreased, implying that continuous malignant tumors might cause malnutrition in mice (**Figure 3G**). To evaluate the effect of treatment modality on each organ (heart, liver, spleen, lung, kidney) and TA muscle, hematoxylin-eosin staining was performed 21 days after plasmid injection. All groups' hearts, kidneys, and TA muscles of all groups did not show any pathological damage (**Figure 3H**). However, spleen tissues were compromised in all groups. The pCombination group was comparatively the least damaged, followed by the pPD-1-scFv and pCTLA-4-scFv groups, which were both more severely damaged than the control groups (MC & pSPsig). In liver tissues, minor infiltrated inflammatory cells were seen in the treatment groups, with mild pathological changes (Figure S4). The lesion did not cause abnormal liver function, as is evident from the biochemical results (**Figure 3E**, **3F**). In general, the common blood and biochemical indices of the treatment groups were close to the reference values, indicating that the treatment could reduce abnormalities in various indices and splenic lesions caused by the tumor while not producing any additional toxic side effects.

Intramuscular pDNA-expressed immunomodulatory scFv combination remolds the tumor immune microenvironment

Next, we explored the immunological changes in the tumor microenvironment caused by intramuscular administration of pPD-1-scFv and pCTLA-4-scFv. In the control group, the B16F0 melanoma model mice received pSPsig injection. Blood and tumors were collected 14 days later, then immune cells were examined using immunohistochemistry and flow cytometry, and the cytokines IFN-γ and TNF-α were measured in mouse blood using an enzyme-linked immunosorbent assay (ELISA). Both monotherapy (pPD-1-scFv & pCTLA-4-scFv) and combined therapy (pCombination) increased the percentage of infiltrating $CD3^+$ T cells as compared to pSPsig treatment, with significant difference between pCombination and other groups and no difference between two monotherapy groups (**Figure 4A**, **4B**). Monotherapy increased the proportion of apoptotic tumor cells by terminal deoxynucleotidyl transferase-mediated nick and labeling (TUNEL) detection. In contrast, more apoptotic tumor cells were detected in the combination group (**Figure 4C**, **4D**), which was consistent with the differences in infiltrating T cells (**Figure 4A**, **4B**).

In addition, we analyzed the presence of T cell subsets within the tumors. The three treatment groups had a significantly higher proportion of $CD8^+$ cytotoxic T cells and $CD4^+$ helper T cells than the control group, but there was no significant difference among the pCombination and

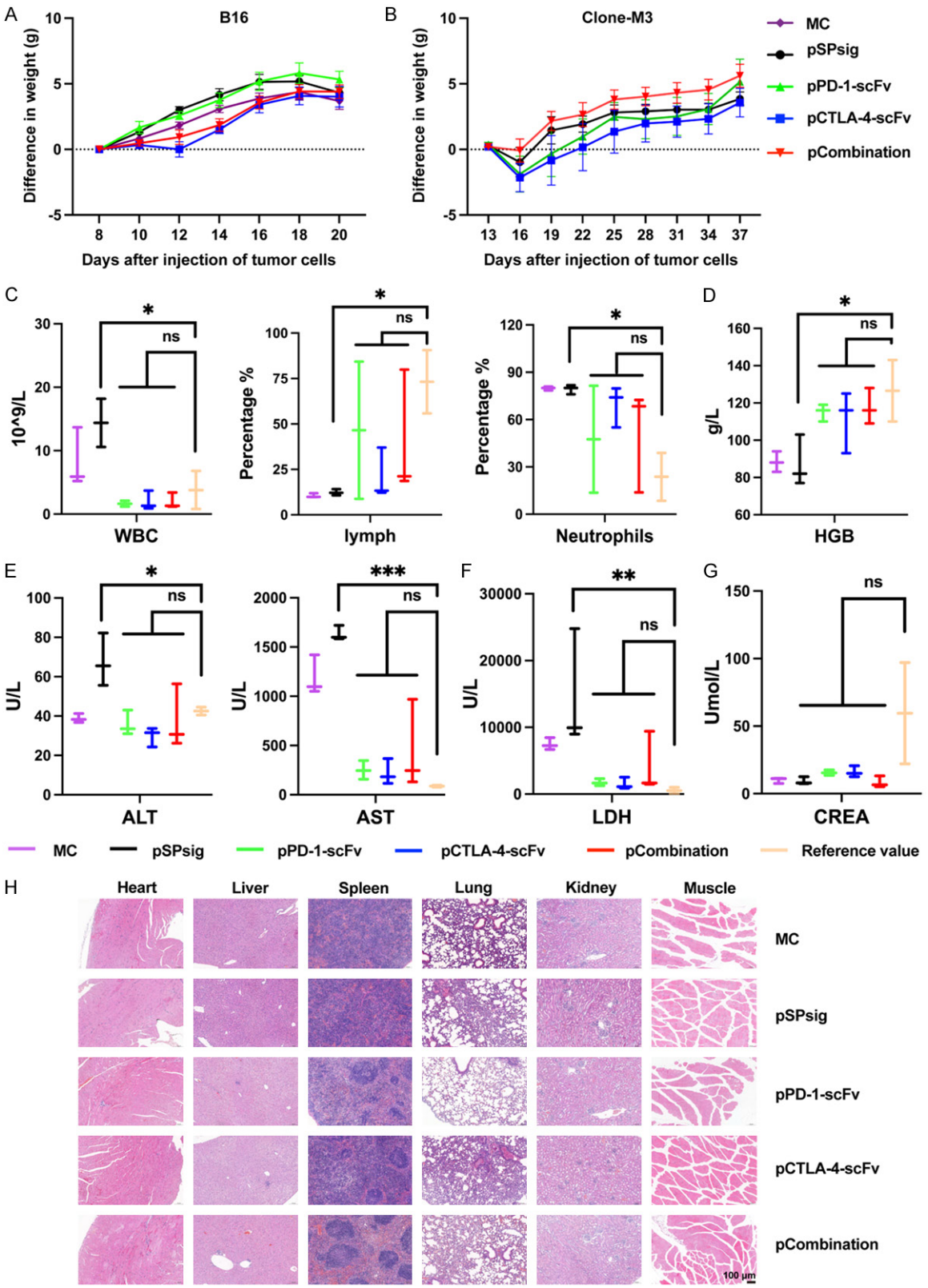

Figure 3. Safety assessment of pPD-1-scFv and pCTLA-4-scFv combination for the treatment of melanoma. A, B. Weight changes in B16F0 and Clone-M3 melanoma mice models. C, D. Routine blood test values of mice, including WBC, lymph, neutrophils, and HGB, in different treatment groups. E-G. Blood chemistry values reflecting liver function and the effect of tumor progression on mice, including ALT, AST, LDH, and CREA, in different treatment groups.

H. Hematoxylin and eosin staining of mouse organs 21 days after plasmid injection. Scale: 100 μm. WBC: white blood cell (leukocyte); HGB: hemoglobin; ALT: glutamic pyruvic transaminase; AST: glutamic oxaloacetic transaminase; LDH: lactate dehydrogenase; CREA: creatinine. Data were presented as the mean ± SD. Data were compared with one-way ANOVA. *P < 0.05, **P < 0.01, and ***P < 0.001.

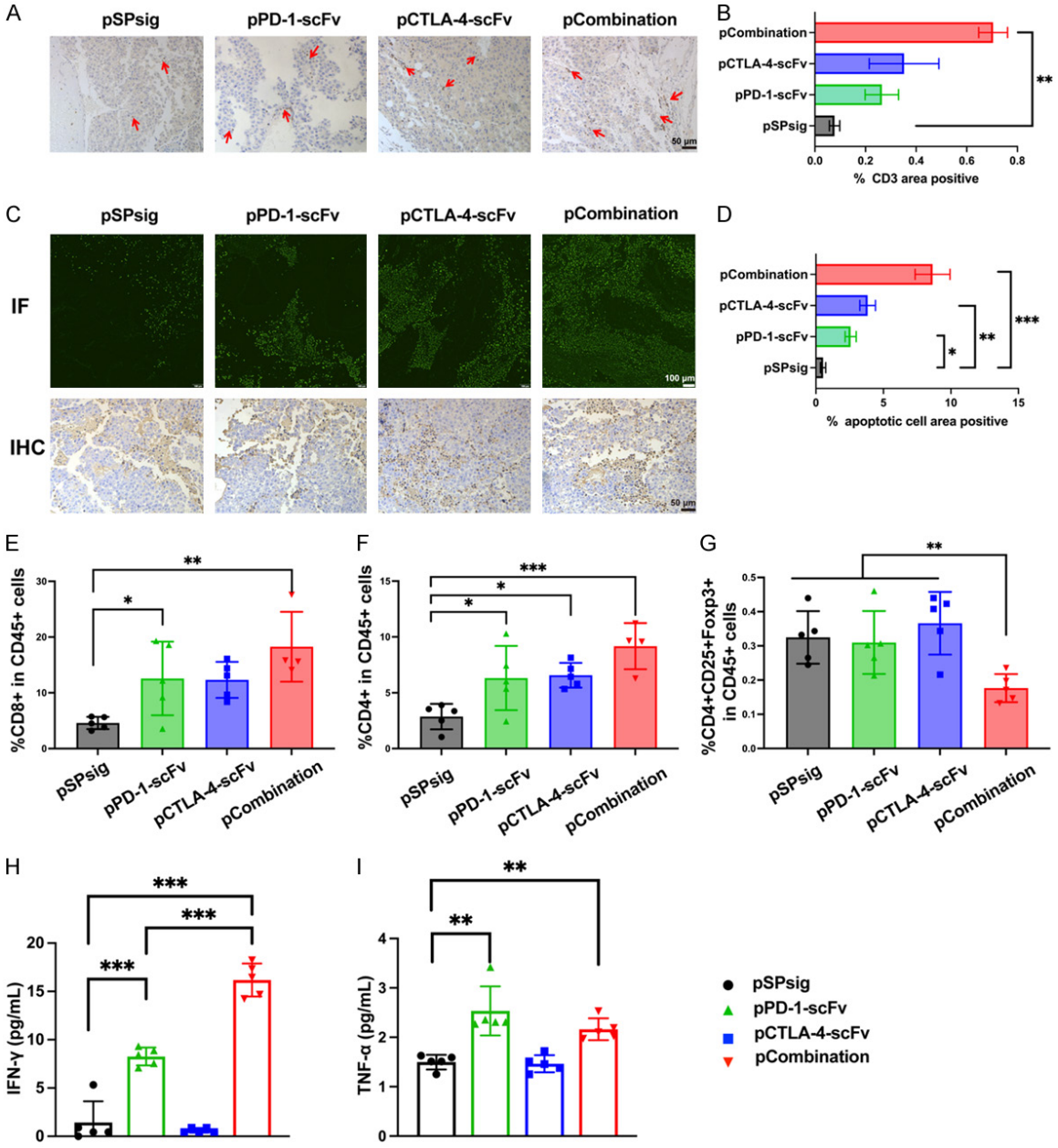

Figure 4. Effects of pDNA-expressed ICI scFvs on tumor immune microenvironment. A. Immunohistochemical staining for CD3$^+$ tumor-infiltrating lymphocytes (TIL; brown) in B16 tumor tissue after different treatments. Scale: 50 μm. B. Percentage of TILs area following the immunostaining of cells with anti-CD3 in tumor tissues. C. Representative TUNEL staining of B16 subcutaneous tumors in different treatment groups. Scale: 100 μm (IF) and 50 μm (IHC). D. Quantification of apoptosis following TUNEL staining by apoptotic index. In another parallel experiment, 14 days after treatment, B16 tumors were harvested and processed into single-cell suspensions, and TILs were analyzed by flow cytometry. N = 5. E. The percentage of cytotoxic CD8$^+$ T cells. F. The percentage of helper CD4$^+$ T cells. G. The percentage of regulatory T cells. H. Concentration of IFN-γ in the serum of B16 melanoma mice. I. Concentration of TNF-α. IFN-γ: interferon γ; TNF-α: tumor necrosis factor α. Data were plotted as the mean ± SD. Data from all treatment groups were compared with one-way ANOVA. *P < 0.05, **P < 0.01, and ***P < 0.001.

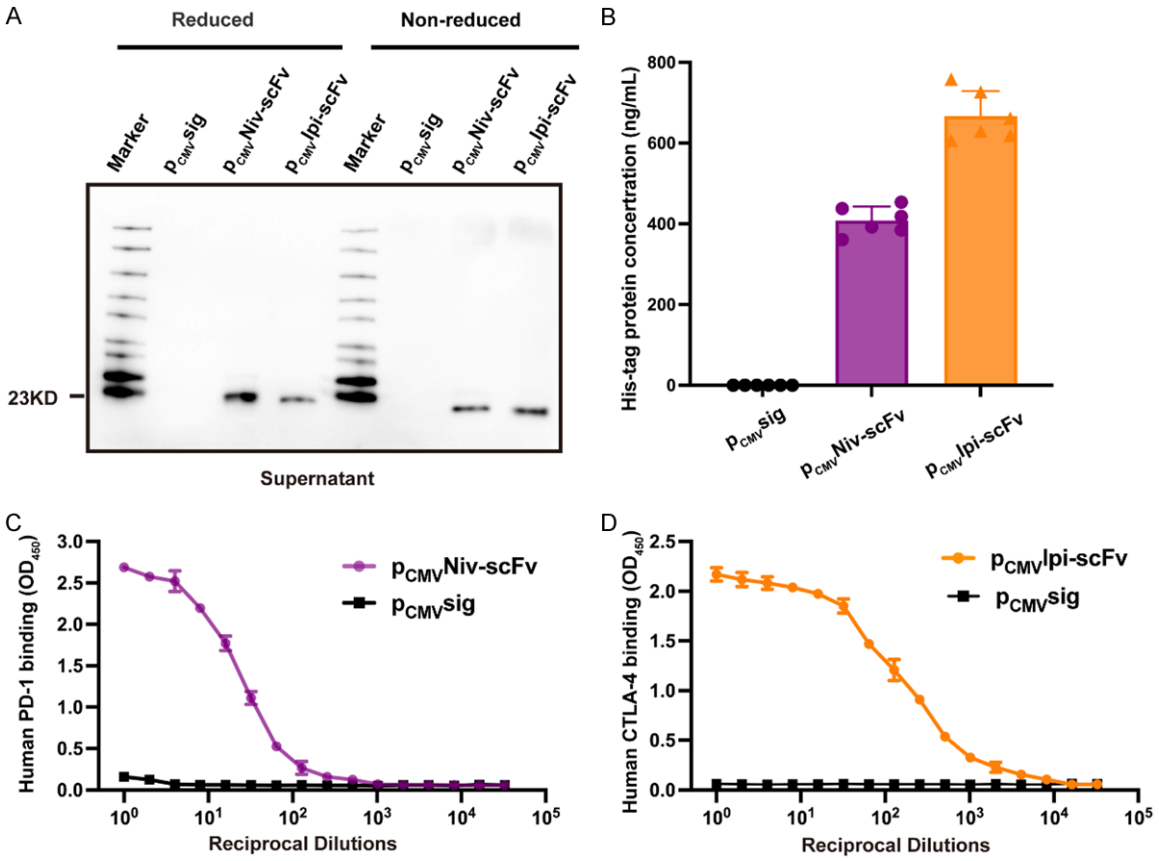

Figure 5. Expression and binding capability of Niv scFv and Ipi scFv *in vitro*. HEK293T cells were transfected with 2.5 μg/well of p_{CMV}sig, p_{CMV}Niv-scFv, and p_{CMV}Ipi-scFv. The supernatants were harvested 48 h later. (A) Western blot analysis of scFvs in cell supernatants under reduced (left) and non-reduced (right) conditions. (B) Quantitative ELISA assay of scFv levels in supernatants. Binding capability of Niv-scFv to human PD-1 protein (C) and Ipi-scFv to human CTLA-4 protein (D), measured by ELISA in cell supernatants. Error bars indicated mean ± SD.

monotherapy groups (**Figure 4E**, **4F**). The overall percentages of $CD8^+$ and $CD4^+$ were still higher in the combination group and more importantly, tumors treated with the pCombination had a significantly lower proportion of regulatory T cells (**Figure 4G**). These results indicated that effective anti-tumor immune responses were evoked and the immunosuppressive tumor microenvironment was improved using the pDNA-based PD-1 and CTLA-4 scFv immunotherapies. Meanwhile, pCombination treatment resulted in the most apparent increase of IFN-γ and TNF-α levels (**Figure 4H**, **4I**). Splenocytes of treated mice were analyzed using flow cytometry to determine whether the pPD-1-scFv and pCTLA-4-scFv treatments also evoked a significant systemic immune activation, which had the possibility to result in adverse events. The percentage of specific immunological T cell subpopulations in the spleen was not altered by any of the therapies (Figure S5), illustrating the biosafety of these therapies again.

Intramuscular pDNA-expressed nivolumab and ipilimumab scFv combination cause significant tumor regressions in humanized mouse melanoma models

In a syngeneic mouse model of melanoma, intramuscular delivery of pDNA to express immune check inhibitors *via* the L/E/G method has shown significant therapeutic effects. Here, combined administration of pDNA encoding clinical Nivolumab (Niv) scFv and Ipilimumab (Ipi) scFv was carried out to examine whether this novel gene therapy system can be applied to human melanoma therapy. Specific bands corresponding to the Niv-scFv and Ipi-scFv were identified in the supernatant of HEK293T cells 48 hours after pDNA transfection under reduced and non-reduced conditions (**Figure 5A**). The concentrations of secreted scFv in

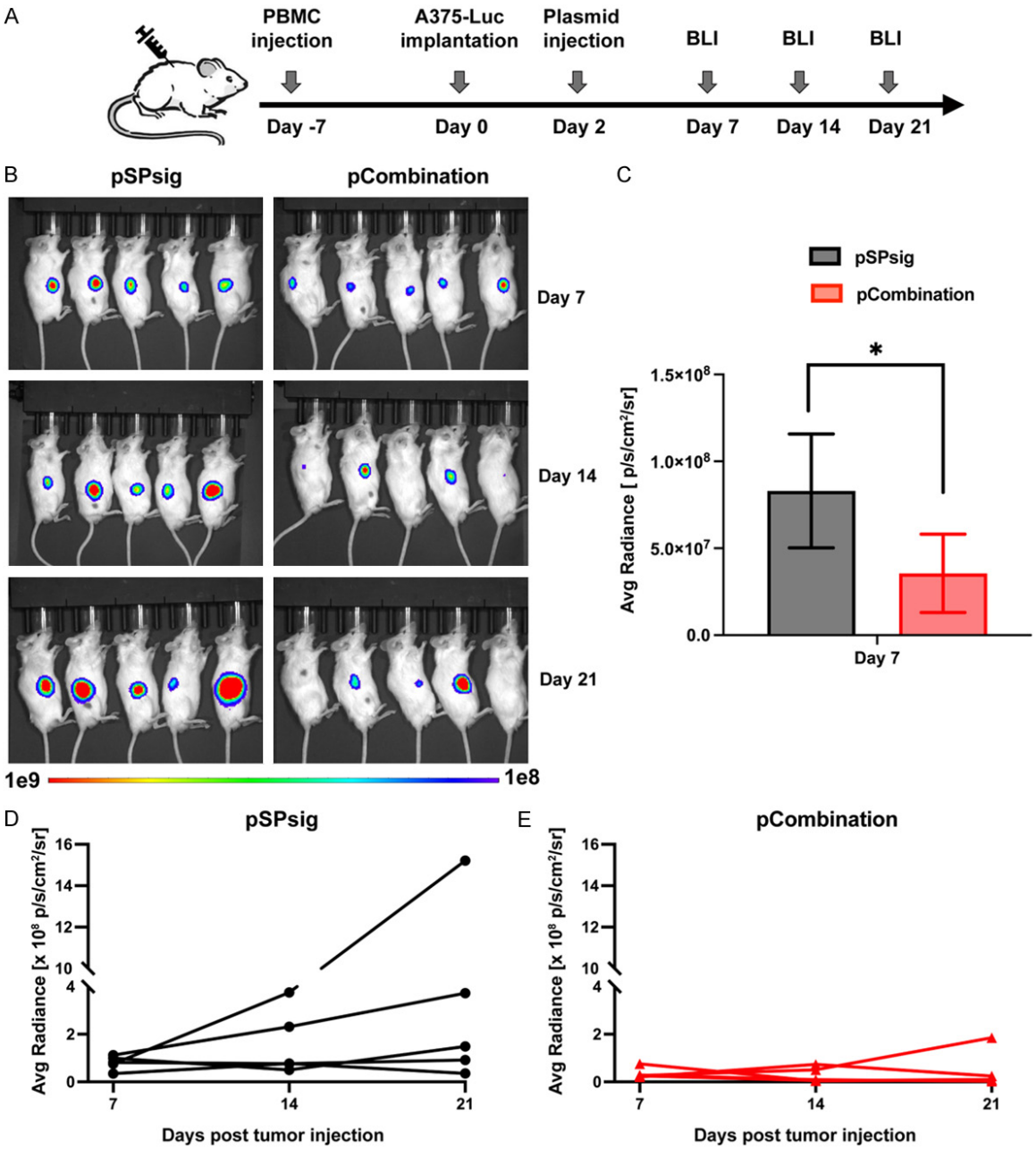

Figure 6. The effectiveness of pDNA-expressed Nivolumab and Ipilimumab scFvs in the A375 xenograft model mice. (A) Schedule of human melanoma cell A375 xenograft model experiment in NOD/scid/IL2rg$^{-/-}$ mice. BLI: Bioluminescence imaging. N = 5. (B) BLI of NOD/scid/IL2rg$^{-/-}$ mice implanted A375-luciferase cells (A375-Luc) followed pSPsig and pCombination (pNiv-scFv & pIpi-scFv) treatment. N = 5. (C) Average radiance quantification (p/s/cm^2/sr) of BLI at day 7. The tumor average radiance trend in the pSPsig (D) and pCombination (E) groups. Error bars indicated mean ± SD. Data from both treatment groups were compared with a t-test. *$P < 0.05$.

supernatants were determined to be 407.5 ng/mL for Niv-scFv and 666.3 ng/mL for Ipi-scFv (**Figure 5B**). Meanwhile, ELISA-binding studies demonstrated that Niv-scFv and Ipi-scFv in supernatants had specific and high affinity to human PD-1 and CTLA-4, respectively (**Figure 5C** and **5D**). The pNiv-scFv and pIpi-scFv were able to express and secrete functional Niv-scFv and Ipi-scFv correctly.

The antitumor effects of this therapeutic system were verified in a mouse xenograft model implanted with A375-Luciferase cells (**Figure 6A**). Human leukocytes were shown to prolifer-

ate in NOD/scid/IL2rg$^{-/-}$ mice by testing human CD45^{+} cells in mice blood samples two weeks and three weeks after PBMC injection (Figure S6). Tumor burdens were calculated by averaging the bioluminescence intensity of 5 mice in each group to evaluate the therapeutic effect. Although tumors were stably detectable 7 days after A375-Luciferase cell inoculation in both groups, there was a substantial difference in tumor size between the groups due to the administration of pCombination on day 2 (**Figure 6B**). The tumor average radiance of the pCombination group was significantly less than that in the control group on day 7 (**Figure 6C**). Subsequently, the pCombination group showed significantly delayed tumor growth in comparison to the control group. Importantly, 2/5 mice in the pCombination group had no detectable tumor on day 21 (**Figure 6D**, **6E**). Altogether, the results illustrated that the novel gene therapy system had an effective therapeutic impact on the humanized mouse model of melanoma.

Discussion

Most of the antibody immunotherapy approaches currently developed for cancer are based on antibody drugs that are directly infused into the human body after production *in vitro*, which requires multiple or continuous injections using a syringe pump to maintain the therapeutic effect of the antibodies. There are several limitations to the widespread use of antibody immunotherapy, such as the complexity of mass production of antibody drugs in the factory, the time and effort required for purification, the infection and patients' psychological problems associated with multiple injections, and the increased cost of patient treatment. Direct *in vivo* expression of antibodies using viruses, mRNA, and DNA offers a solution to some of these issues.

While antibody gene transfer *via* muscle has been reported for tumor treatment, few studies have focused on multiple plasmid delivery for combination therapy. The plasmid-encoded anti-CTLA-4 and anti-PD-1 IgG-antibodies have been studied in pharmacokinetics, and pharmacodynamics when applied alone and in combination, administered *via* intramuscular or intra-tumor electro-transfection [23, 24]. However, because the two medications have different modes of action, which act on separate lymphocyte subtypes and in different places, concurrent treatment increases the frequency of side effects, particularly colitis and rash. The most notable of the adverse effects, small bowel colitis, was associated with the Fc-effector of CTLA4 antibodies [21, 22]. In addition, some studies concluded that CTLA4 antibody requires an Fc-effector for clearance of Treg [25, 26]. In terms of antitumor effects, the possible association between irAEs induced by checkpoint inhibitors and clinical benefit has not been fully elucidated. Since the antibody gene transfer strategy through muscle will produce antibodies from muscle cells continuously, the concentration of antibodies *in vivo* will continue to rise over time, we believe that the expressed antibodies need to be cleared somewhat rapidly to reduce the adverse events associated with combination therapy for safety reasons. The majority of IgG-type antibodies employed in DMAb (DNA-encoded monoclonal antibody) research have a high molecular weight and a prolonged half-life i*n vivo* [27]. Moreover, the question of how the light and heavy chains are linked comes up when the gene for an IgG-type antibody is fused to the vector.

Previous studies obtained antibody expression *in vivo* by introducing P2A or IRES to link the light and heavy chains through a single promoter. However, cleavage of the 2A peptide leaves a 20 amino acid polypeptide in the tail of the former protein and a redundant proline at the N-terminal end of the latter protein. These residual amino acids may affect the function of the proteins and have the potential risk of initiating an immune response. IRES ligation can cause an imbalance in the expression of light and heavy chains, and overexpression of one of them may result in additional toxicity [28-30]. Given the factors above, the DNA expressed *in vivo* for combination therapy was determined to be the sequence encoding the variable region of the light and heavy chains of PD-1 and CTLA-4 antibodies, joined by a flexible linker and built on a plasmid vector. The scFv mainly assumes the role of antigen binding, and its gene sequence is a complete sequence that does not require P2A or IRES [17]. However, there is no optimal stipulation or choice for constructing plasmids used for expression of antibodies *in vivo*.

In the DMAb strategy, electroporation and gene delivery materials are essential for determining the efficiency of gene expression. In this study, L64 was added to disrupt the cell membrane structure and increase muscle cell permeability to promote plasmid penetration, whereas EGCG was added to compress and protect the plasmids [14, 31]. We also used muscle-specific promoters to drive gene expression and performed muscle delivery of the scFv-ICI plasmid at an optimized electroporation voltage [15, 32]. Herein, the antibody gene expression was increased in multiple ways to achieve melanoma treatment in mice. As current studies focus on mouse models, our muscle-specific promoters were evaluated using murine muscle cells. Nevertheless, studies on human muscle cells are needed to improve the DMAb clinical development strategies [32].

The therapeutic effects of the Clone-M3 mouse model demonstrated that this strategy has a more prominent impact on slow-growing tumors. This strategy may also be used as adjuvant maintenance therapy and have better efficacy in human tumors. We extended the study of in vivo production of ICIs for melanoma to the CDX model [23]. During the bioluminescence of A375-CDX mice, comparable experimental results were observed as in the B16 model, with substantial variations in tumor volume between the combined treatment group and the control group, even though animals were able to develop tumors simultaneously. It suggested that the intervention performed by this strategy at an early stage of the cancer has an outstanding effect, which is the key to prolonging survival. In the combination group, we found a complete disappearance of tumors with a better efficacy observed in the CDX model than in the B16 model, probably because murine and human antibodies do not have the same binding capacity for their respective antigens. The variation in binding capacity could be attributable to the structure or gene sequence. This would imply that the antibody binding capacity and expression concentration should be included in the optimization settings for this method.

More conditions need to be considered for multiple antibody combination therapies. And more refined improvements need to be proposed for combination therapy with preserved effects and low toxicity based on DMAb strategies in the future. Tumor-conditional antibodies are now being made so that the effects of the antibody are more likely to be focused at the site of the tumor [33]. It is important to extensively explore developing DMAb strategies, such as *in vivo* modulation of antibody expression to let patients self-regulate, which can be studied with a tumorigenesis mechanism. In addition, using the principle of exon splicing regulation, the timing of protein expression *in vivo* can be induced by oral bioavailable and human-used to achieve better biosafety [34]. These will make therapeutic manipulation easier for doctors and give cancer patients relatively cheaper, more effective, and less complicated treatment. The good correlation between the amount of plasmid injected and antibody levels in circulation after muscle electroporation allows the DNA dose to be injected to be precisely calculated to obtain the desired therapeutic effect. This strategy can regulate the levels of the therapeutic protein according to the needs of each patient by controlling the dose of pDNA. Moreover, the therapeutic effect is prolonged by multiple dosing at intervals over some time [35, 36].

Overall, this study demonstrated that intramuscular administration of muscle-specific promotor-derived immune checkpoint plasmid can effectively combine PD-1 and CTLA-4 scFv for melanoma treatment. Moreover, the therapy exerted outstanding antitumor effects and had a favorable safety profile, and our study promotes the development of immune combination therapies based on intramuscular injection of plasmids.

Acknowledgements

This work was supported by the 1.3.5 Project for Disciplines of Excellence, West China Hospital, Sichuan University (Grant No. ZYJC21043), National Natural Science Foundation of China (31971390), International Cooperative Project of Sichuan Province on Science and Technology Innovation (No. 2021YFH0142), and Social development Science and Technology Project of Sichuan Province on Science and Technology (2023YFS0111).

Disclosure of conflict of interest

None.

Address correspondence to: Dr. Gang Wang, National Engineering Research Center for Biomaterials, Sichuan University, Chengdu 610064, Sichuan, China. ORCID: 0000-0003-3296-3015; E-mail: wgang@scu.edu.cn; Dr. Ming Liu, Department of Medical Oncology/Gastric Cancer Center, West China Hospital, Sichuan University, Chengdu 610041, Sichuan, China. ORCID: 0000-0002-8662-3190; E-mail: liuming629@wchscu.cn

References

[1] Bastian BC. The molecular pathology of melanoma: an integrated taxonomy of melanocytic neoplasia. Annu Rev Pathol 2014; 9: 239-271.

[2] Weiss SA, Wolchok JD and Sznol M. Immunotherapy of melanoma: facts and hopes. Clin Cancer Res 2019; 25: 5191-5201.

[3] Larkin J, Chiarion-Sileni V, Gonzalez R, Grob JJ, Cowey CL, Lao CD, Schadendorf D, Dummer R, Smylie M, Rutkowski P, Ferrucci PF, Hill A, Wagstaff J, Carlino MS, Haanen JB, Maio M, Marquez-Rodas I, McArthur GA, Ascierto PA, Long GV, Callahan MK, Postow MA, Grossmann K, Sznol M, Dreno B, Bastholt L, Yang A, Rollin LM, Horak C, Hodi FS and Wolchok JD. Combined nivolumab and ipilimumab or monotherapy in untreated melanoma. N Engl J Med 2015; 373: 23-34.

[4] Rini BI, Battle D, Figlin RA, George DJ, Hammers H, Hutson T, Jonasch E, Joseph RW, McDermott DF, Motzer RJ, Pal SK, Pantuck AJ, Quinn DI, Seery V, Voss MH, Wood CG, Wood LS and Atkins MB. The society for immunotherapy of cancer consensus statement on immunotherapy for the treatment of advanced renal cell carcinoma (RCC). J Immunother Cancer 2019; 7: 354.

[5] Paz-Ares LG, Ramalingam SS, Ciuleanu TE, Lee JS, Urban L, Caro RB, Park K, Sakai H, Ohe Y, Nishio M, Audigier-Valette C, Burgers JA, Pluzanski A, Sangha R, Gallardo C, Takeda M, Linardou H, Lupinacci L, Lee KH, Caserta C, Provencio M, Carcereny E, Otterson GA, Schenker M, Zurawski B, Alexandru A, Vergnenegre A, Raimbourg J, Feeney K, Kim SW, Borghaei H, O'Byrne KJ, Hellmann MD, Memaj A, Nathan FE, Bushong J, Tran P, Brahmer JR and Reck M. First-line nivolumab plus ipilimumab in advanced NSCLC: 4-year outcomes from the randomized, open-label, phase 3 CheckMate 227 part 1 trial. J Thorac Oncol 2022; 17: 289-308.

[6] Wolchok JD, Chiarion-Sileni V, Gonzalez R, Grob JJ, Rutkowski P, Lao CD, Cowey CL, Schadendorf D, Wagstaff J, Dummer R, Ferrucci PF, Smylie M, Butler MO, Hill A, Márquez-Rodas I, Haanen JBAG, Guidoboni M, Maio M, Schöffski P, Carlino MS, Lebbé C, McArthur G, Ascierto PA, Daniels GA, Long GV, Bas T, Ritchings C, Larkin J and Hodi FS. Long-term outcomes with nivolumab plus ipilimumab or nivolumab alone versus ipilimumab in patients with advanced melanoma. J Clin Oncol 2022; 40: 127-137.

[7] Fang J, Yi S, Simmons A, Tu GH, Nguyen M, Harding TC, VanRoey M and Jooss K. An antibody delivery system for regulated expression of therapeutic levels of monoclonal antibodies in vivo. Mol Ther 2007; 15: 1153-1159.

[8] Rybakova Y, Kowalski PS, Huang Y, Gonzalez JT, Heartlein MW, DeRosa F, Delcassian D and Anderson DG. mRNA delivery for therapeutic anti-HER2 antibody expression in vivo. Mol Ther 2019; 27: 1415-1423.

[9] Vijayakumar G, Palese P and Goff PH. Oncolytic newcastle disease virus expressing a checkpoint inhibitor as a radioenhancing agent for murine melanoma. EBioMedicine 2019; 49: 96-105.

[10] Bommareddy PK, Shettigar M and Kaufman HL. Integrating oncolytic viruses in combination cancer immunotherapy. Nat Rev Immunol 2018; 18: 498-513.

[11] Wang C, Zhang Y and Dong Y. Lipid nanoparticle-mRNA formulations for therapeutic applications. Acc Chem Res 2021; 54: 4283-4293.

[12] Hartikka J, Sukhu L, Buchner C, Hazard D, Bozoukova V, Margalith M, Nishioka WK, Wheeler CJ, Manthorp M and Sawdey M. Electroporation-facilitated delivery of plasmid DNA in skeletal muscle: plasmid dependence of muscle damage and effect of poloxamer 188. Mol Ther 2001; 4: 407-415.

[13] Daud AI, DeConti RC, Andrews S, Urbas P, Riker AI, Sondak VK, Munster PN, Sullivan DM, Ugen KE, Messina JL and Heller R. Phase I trial of interleukin-12 plasmid electroporation in patients with metastatic melanoma. J Clin Oncol 2008; 26: 5896-5903.

[14] He Y, Liu Y, Sun Z, Han F, Tang JZ, Gao R and Wang G. The proper strategy to compress and protect plasmid DNA in the Pluronic L64-electropulse system for enhanced intramuscular gene delivery. Regen Biomater 2019; 6: 289-298.

[15] Liu S, Ma L, Tan R, Lu Q, Geng Y, Wang G and Gu Z. Safe and efficient local gene delivery into skeletal muscle via a combination of pluronic L64 and modified electrotransfer. Gene Ther 2014; 21: 558-565.

[16] Chen W, Yuan Y and Jiang X. Antibody and antibody fragments for cancer immunotherapy. J Control Release 2020; 328: 395-406.

[17] Lou H and Cao X. Antibody variable region engineering for improving cancer immunotherapy. Cancer Commun (Lond) 2022; 42: 804-827.
[18] Ramos-Casals M, Brahmer JR, Callahan MK, Flores-Chávez A, Keegan N, Khamashta MA, Lambotte O, Mariette X, Prat A and Suárez-Almazor ME. Immune-related adverse events of checkpoint inhibitors. Nat Rev Dis Primers 2020; 6: 38.
[19] Martins F, Sofiya L, Sykiotis GP, Lamine F, Maillard M, Fraga M, Shabafrouz K, Ribi C, Cairoli A, Guex-Crosier Y, Kuntzer T, Michielin O, Peters S, Coukos G, Spertini F, Thompson JA and Obeid M. Adverse effects of immune-checkpoint inhibitors: epidemiology, management and surveillance. Nat Rev Clin Oncol 2019; 16: 563-580.
[20] Uhara H, Kiyohara Y, Uehara J, Fujisawa Y, Takenouchi T, Otsuka M, Uchi H, Fukushima S, Minami H, Hatsumichi M and Yamazaki N. Five-year survival with nivolumab in previously untreated Japanese patients with advanced or recurrent malignant melanoma. J Dermatol 2021; 48: 592-599.
[21] Bauché D, Mauze S, Kochel C, Grein J, Sawant A, Zybina Y, Blumenschein W, Yang P, Annamalai L, Yearley JH, Punnonen J, Bowman EP, Chackerian A and Laface D. Antitumor efficacy of combined CTLA4/PD-1 blockade without intestinal inflammation is achieved by elimination of FcγR interactions. J Immunother Cancer 2020; 8: e001584.
[22] Lo BC, Kryczek I, Yu J, Vatan L, Caruso R, Matsumoto M, Sato Y, Shaw MH, Inohara N, Xie Y, Lei YL, Zou W and Núñez G. Microbiota-dependent activation of CD4+ T cells induces CTLA-4 blockade-associated colitis via Fcγ receptors. Science 2024; 383: 62-70.
[23] Jacobs L, De Smidt E, Geukens N, Declerck P and Hollevoet K. DNA-based delivery of checkpoint inhibitors in muscle and tumor enables long-term responses with distinct exposure. Mol Ther 2020; 28: 1068-1077.
[24] Jacobs L, Yshii L, Junius S, Geukens N, Liston A, Hollevoet K and Declerck P. Intratumoral DNA-based delivery of checkpoint-inhibiting antibodies and interleukin 12 triggers T cell infiltration and anti-tumor response. Cancer Gene Ther 2022; 29: 984-992.
[25] Ha D, Tanaka A, Kibayashi T, Tanemura A, Sugiyama D, Wing JB, Lim EL, Teng KWW, Adeegbe D, Newell EW, Katayama I, Nishikawa H and Sakaguchi S. Differential control of human Treg and effector T cells in tumor immunity by Fc-engineered anti-CTLA-4 antibody. Proc Natl Acad Sci U S A 2019; 116: 609-618.
[26] Gan X, Shan Q, Li H, Janssens R, Shen Y, He Y, Chen F, van Haperen R, Drabek D, Li J, Zhang Y, Zhao J, Qin B, Jheng MJ, Chen V, Wang J, Rong Y and Grosveld F. An anti-CTLA-4 heavy chain-only antibody with enhanced T(reg) depletion shows excellent preclinical efficacy and safety profile. Proc Natl Acad Sci U S A 2022; 119: e2200879119.
[27] Peng F, Wang Y, Zhao J, Liu H, Liu Z, Ding K, Zhang H and Fu R. Gene therapy with B-cell maturation antigen/CD3 bispecific antibody encoding plasmid DNA for treating multiple myeloma. Br J Haematol 2023; 201: 417-421.
[28] Kim H, Danishmalik SN, Hwang H, Sin JI, Oh J, Cho Y, Lee H, Jeong M, Kim SH and Hong HJ. Gene therapy using plasmid DNA-encoded anti-HER2 antibody for cancers that overexpress HER2. Cancer Gene Ther 2016; 23: 341-347.
[29] Khoshnejad M, Patel A, Wojtak K, Kudchodkar SB, Humeau L, Lyssenko NN, Rader DJ, Muthumani K and Weiner DB. Development of novel DNA-encoded PCSK9 monoclonal antibodies as lipid-lowering therapeutics. Mol Ther 2019; 27: 188-199.
[30] Muthumani K, Marnin L, Kudchodkar SB, Perales-Puchalt A, Choi H, Agarwal S, Scott VL, Reuschel EL, Zaidi FI, Duperret EK, Wise MC, Kraynyak KA, Ugen KE, Sardesai NY, Joseph Kim J and Weiner DB. Novel prostate cancer immunotherapy with a DNA-encoded anti-prostate-specific membrane antigen monoclonal antibody. Cancer Immunol Immunother 2017; 66: 1577-1588.
[31] Chen J, Luo J, Zhao Y, Pu L, Lu X, Gao R, Wang G and Gu Z. Increase in transgene expression by pluronic L64-mediated endosomal/lysosomal escape through its membrane-disturbing action. ACS Appl Mater Interfaces 2015; 7: 7282-7293.
[32] Liu Y, He Y, Wang Y, Liu M, Jiang M, Gao R and Wang G. Synthetic promoter for efficient and muscle-specific expression of exogenous genes. Plasmid 2019; 106: 102441.
[33] Pai CS, Simons DM, Lu X, Evans M, Wei J, Wang YH, Chen M, Huang J, Park C, Chang A, Wang J, Westmoreland S, Beam C, Banach D, Bowley D, Dong F, Seagal J, Ritacco W, Richardson PL, Mitra S, Lynch G, Bousquet P, Mankovich J, Kingsbury G and Fong L. Tumor-conditional anti-CTLA4 uncouples antitumor efficacy from immunotherapy-related toxicity. J Clin Invest 2019; 129: 349-363.
[34] Cripe TP, Hutzen B, Currier MA, Chen CY, Glaspell AM, Sullivan GC, Hurley JM, Deighen MR, Venkataramany AS, Mo X, Stanek JR, Miller AR, Wijeratne S, Magrini V, Mardis ER, Mendell JR, Chandler DS and Wang PY. Leveraging gene therapy to achieve long-term continuous or controllable expression of biotherapeutics. Sci Adv 2022; 8: eabm1890.

[35] Deng L, Yang P, Li C, Xie L, Lu W, Zhang Y, Liu M and Wang G. Prolonged control of insulin-dependent diabetes via intramuscular expression of plasmid-encoded single-strand insulin analogue. Genes Dis 2022; 10: 1101-1113.

[36] Xie L, Lu W, Zhang Y, Deng L, Liu M, Gao H, Xie C and Wang G. Glucose-activated switch regulating insulin analog secretion enables long-term precise glucose control in mice with type 1 diabetes. Diabetes 2023; 72: 703-714.

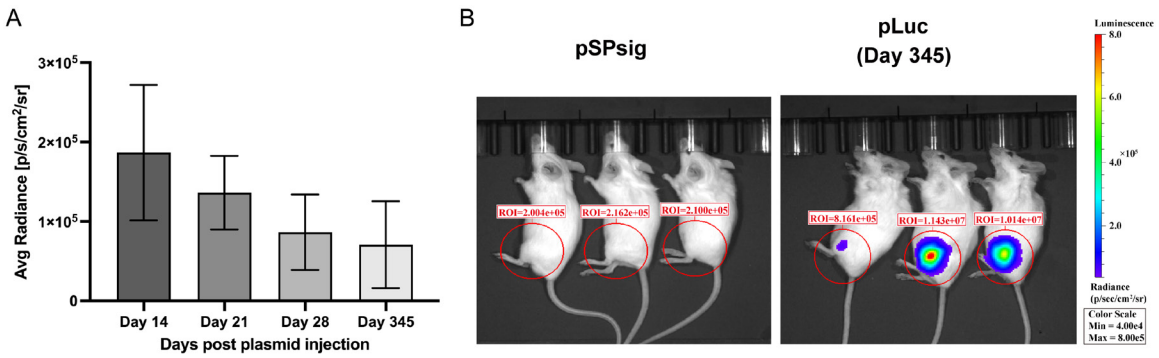

Figure S1. Luciferase expression in mice receiving intramuscular administration of pLuc with L/E/G technique. A. Luciferase expression in different time. B. Bioluminescence image in mice receiving intramuscular administration of pSPsig and pLuc at day 345. ROI = Total Flux (p/s). N = 3.

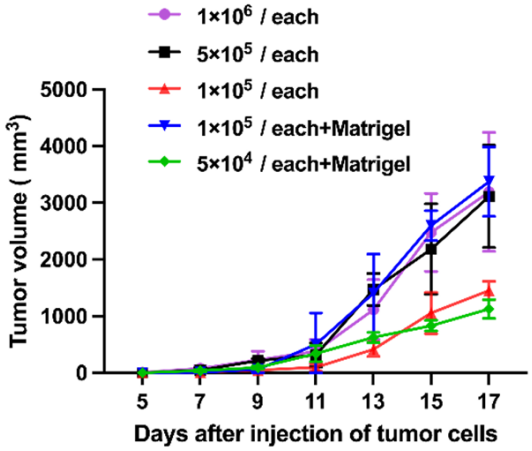

Figure S2. Optimization of the inoculation number of B16 cells in C57BL/6 mice. N = 5.

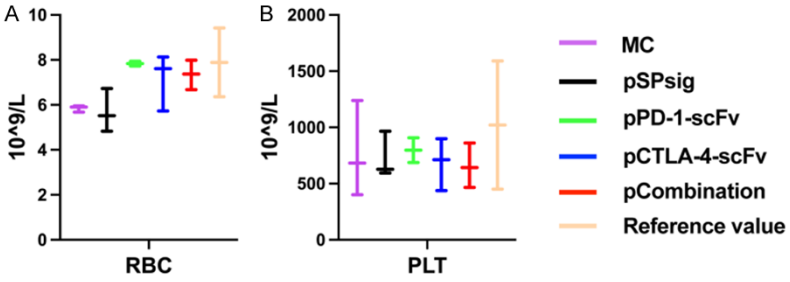

Figure S3. Routine blood test values of RBC and PLT in different groups. N = 3. RBC: red blood cell; PLT: platelet.

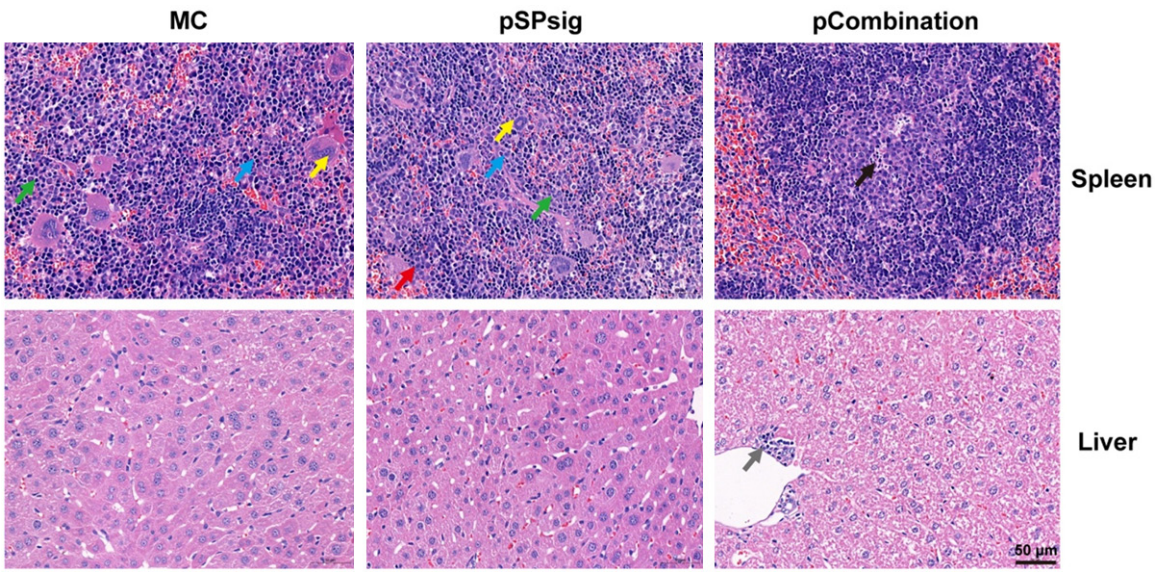

Figure S4. Hematoxylin and eosin staining of spleen and liver tissue sections (× 400). Necrosis of lymphocytes (black arrowhead), megakaryocytic (yellow arrowhead), mitosis (blue arrowhead), granulocytes (green arrowhead), erythroid cells (red arrowhead), lymphocytes (grey arrowhead). Scale bar: 50 μm.

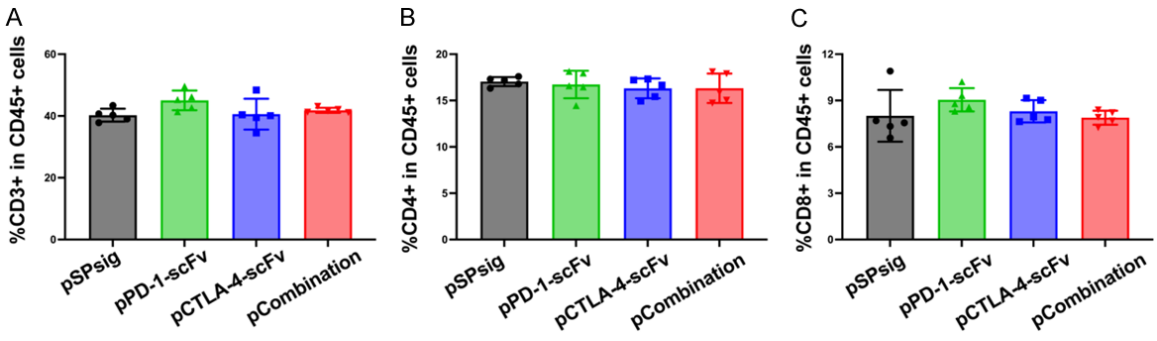

Figure S5. Effect of pDNA-expressed ICI scFvs on splenocytes. A. The percentage of $CD3^+$ T cells. B. The percentage of helper $CD4^+$ T cells. C. The percentage of cytotoxic $CD8^+$ T cells. N = 5.

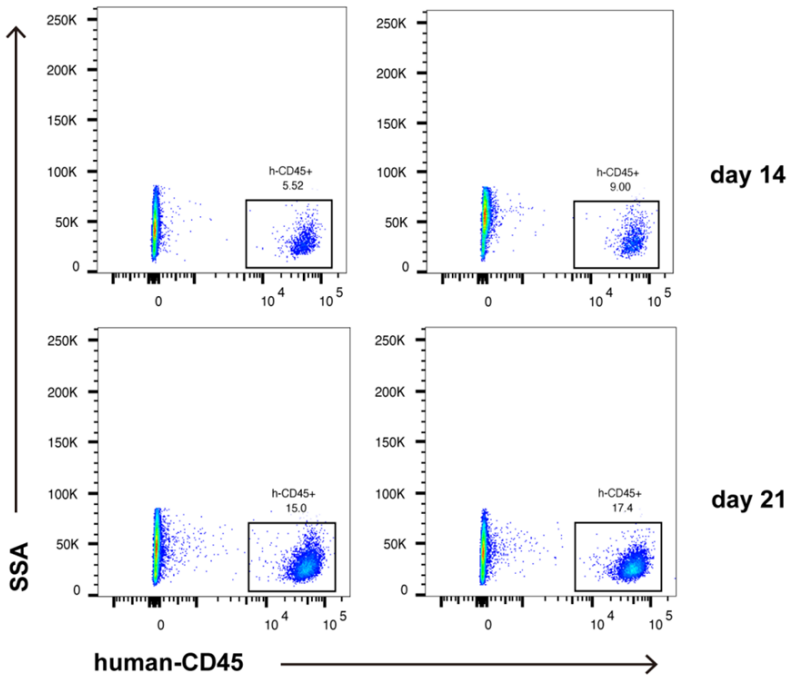

Figure S6. Identification of Hu-PBL-SCID model. Analysis of human CD45$^+$ cells in the blood of NOD/scid/IL2rg$^{-/-}$ mice by flow cytometry on days 14 and 21 after PBMC injection. N = 2.